Optical pumping of ^{29}Si nuclear spins in bulk silicon at high magnetic field and liquid helium temperature

Anne S. Verhulst,* Ileana G. Rau, and Yoshihisa Yamamoto†
Quantum Entanglement Project, ICORP, JST, E.L. Ginzton Laboratory, Stanford University, Stanford, California 94305-4088, USA

Kohei M. Itoh
Department of Applied Physics and Physico-Informatics, Keio University and CREST-JST, Yokohama 223-8522, Japan
(Received 15 December 2004; published 16 June 2005)

High nuclear spin polarization is required for nuclear-spin based quantum computers and it also serves as a probe to investigate electron-nucleus cross-relaxation processes in solids. To increase the ^{29}Si polarization in bulk silicon, we have explored the dynamic-nuclear-polarization capabilities of optical pumping at a temperature of 4 K and a magnetic field of 7 T with a ^{29}Si-enriched sample. The ^{29}Si signals are observed with nuclear-magnetic-resonance spectroscopy. We have demonstrated ^{29}Si polarizations up to 0.25%, nearly an order of magnitude larger than the previous optical-pumping record. Data analysis has stimulated the investigation of above-band-gap excitations. Our preliminary experiments in this regime look promising for further increases in ^{29}Si polarization in the sample volume close to the exposed surface. We have also investigated the dependence of the ^{29}Si polarization on temperature, magnetic field, and doping.

DOI: 10.1103/PhysRevB.71.235206 PACS number(s): 76.70.Fz, 03.67.Lx, 72.25.Fe, 76.60.−k

I. INTRODUCTION

Intensive experimental efforts to fabricate quantum computers have been made over the past few years. After several proof-of-principle demonstrations with liquid-state nuclear-magnetic-resonance (NMR) quantum computers,[1,2] the experimental focus has shifted toward the fabrication of more scalable quantum computers. One promising architecture is the solid-state nuclear-spin-based architecture.[3–5] In the silicon-based proposals of this architecture,[6,7] it is required that the polarization of the ^{31}P nuclear spins and the ^{29}Si nuclear spins, respectively, are larger than 10% for an efficient operation of the quantum computer. Such high nuclear spin polarizations are in sharp contrast with the low thermal-equilibrium values.

Optical pumping in silicon to increase nuclear spin polarizations was first demonstrated in the late 1960s by Lampel.[8] Bagraev *et al.* continued this research[9] and explored in more detail the impact of several parameters, in particular the effect of impurities. Their largest ^{29}Si polarization was 0.03%.[10] The main focus of the semiconductor optical-pumping research, however, has been on gallium arsenide (GaAs), where optical pumping effects are very strong because GaAs is a direct band-gap material.[11] The GaAs research has evolved from an investigation of the optical pumping mechanism in bulk GaAs, to a study of the properties of quantum-confined electrons in GaAs quantum wells and more recently to a study of optical pumping effects in quantum dots.[12,13] In silicon on the other hand no optical pumping research has been pursued for about two decades and the regime of high magnetic fields (>1 T) and liquid helium temperatures has not yet been explored. The recent availability of ^{29}Si-enriched single-crystal silicon,[14–16] which provides an NMR-signal increase of a factor of 20 compared to naturally-abundant silicon, together with the availability of a Ti:Al_2O_3-laser which allows optical excitation below and above the indirect band gap of silicon, motivate the continuation of the optical pumping research in silicon.

We present optical pumping experiments with silicon in a high magnetic field ($B_0=7$ T) and at low temperatures ($T=4$ K). Our largest ^{29}Si polarization so far is 0.25%. We argue that the increase of the ^{29}Si polarization with laser power at a fixed wavelength is due to a better preservation of the non-thermal free-electron spin polarization as the laser power increases. Based on this model, we make predictions about the maximum achievable ^{29}Si polarization and we derive that excitation high above the band gap is promising for practical realizations of large ^{29}Si polarizations. We present data on the ^{29}Si polarization as a function of laser wavelength and preliminary experiments confirm that excitation above the band gap is promising. We also present data on the dependence of the ^{29}Si polarization on temperature, magnetic field, and doping.

II. EXPERIMENTAL SETUP

The light source is a continuous-wave single-frequency Ti:Al_2O_3 laser of Spectra-Physics (Mountain View, California 94043, USA), which has been specially designed for high power emission at long wavelengths. The spectral width of the laser beam is smaller than $\Delta\lambda=15$ GHz. Irradiation of the sample, which is mounted in the holder of an NMR probe, occurs through the top glass plate of the probe and reflections of the laser beam off of this glass plate are used for alignment verification.[17] The laser light is linearly polarized such that electrons (and holes) with zero spin polarization are injected.

The NMR probe is inserted in a continuous-flow cryostat of Oxford Instruments (Abingdon, Oxfordshire 0X13 5QX, United Kingdom), which allows one to cool down the sample to 4 K. A cernox temperature sensor is installed close

to the sample and in good thermal contact with the sample.[17] With a temperature control system, fluctuations of less than $\Delta T = 0.5$ K are achieved at liquid helium temperatures.

The cryostat is located in the bore of a superconducting magnet ($B_0 = 7$ or 2 T, with corresponding ^{29}Si resonance frequencies of $f^{Si}_{Larmor} = 59.58$ MHz and $f^{Si}_{Larmor} = 18.13$ MHz, respectively). The ^{29}Si NMR signals are recorded with a home-built NMR spectrometer. The sign of the NMR signals and of the spin polarization is determined by the orientation of the spin with respect to the external magnetic field. Since the gyromagnetic ratio of ^{29}Si is negative, the thermal equilibrium ^{29}Si polarization is negative.

All samples used in this study are single-crystal silicon and are mounted with the [100] crystal axis parallel to the magnetic field. Naturally-abundant silicon (92.2% ^{28}Si, 4.7% ^{29}Si, 3.1% ^{30}Si) is used for a few experiments. However the small ^{29}Si isotopic content, with ^{29}Si being the only isotope with nonzero spin ($I = 1/2$), results in very weak NMR signals. For most of our experiments, we have therefore used a ^{29}Si-enriched sample with 2.4% ^{28}Si, 96.9% ^{29}Si, and 0.7% ^{30}Si. Since the ^{29}Si content of the ^{29}Si-enriched sample is about 20 times larger than in naturally-abundant silicon, the NMR signals are 20 times larger. The time to obtain an observable ^{29}Si NMR signal can therefore be shortened with a factor of 20, which is very valuable in view of the long ^{29}Si nuclear-spin relaxation times T^{Si}_1 at 4 K. This ^{29}Si-enriched sample has been fabricated as part of a research project. The sample has a cylindrical shape with an approximate diameter of 8 mm and a height of 4.5 mm. A phosphorus content of $1-2\times10^{15}$ cm^{-3} has been measured, as well as an antimony content of less than 10^{14} cm^{-3}. The sample dislocation density is expected to be larger than 10^3 cm^{-2}.

III. SILICON BAND STRUCTURE

Silicon is an indirect band-gap material ($E_{g,\mathrm{ind}} = 1.170$ eV at $T = 4$ K)[18,19] and therefore the band-to-band transitions are phonon-assisted. At $T = 4$ K only transitions with phonon emission occur. The energies of the three dominant phonon reservoirs, assisting band-to–band transitions, are $E_{\mathrm{phonon}} = 18.2$ meV (transverse acoustical—TA), $E_{\mathrm{phonon}} = 55.3$ meV (longitudinal optical—LO), and $E_{\mathrm{phonon}} = 57.5$ meV (transverse optical—TO) for transitions at the band gap.[18] Because photon absorption and emission are three-particle processes, the photon absorption process is weak (long absorption lengths) and the radiative lifetime of electronic carriers is long.

IV. RESULTS AT $\lambda_{\mathrm{photon}} = 1024.8$ NM AS A FUNCTION OF LASER POWER

To gain insight in the optical pumping mechanism, the ^{29}Si NMR-signal intensity has been recorded as a function of laser power for our ^{29}Si-enriched sample at $T = 4$ K and $B_0 = 7$ T. The laser wavelength is $\lambda_{\mathrm{photon}} = 1024.8$ nm ($E_{\mathrm{photon}} = 1.210$ eV), which corresponds to the above-band-gap transition with TA-phonon emission. This wavelength is chosen because of the experimentally favorable condition that the largest ^{29}Si NMR signals are obtained at this wavelength for short-duration optical pumping experiments (see Sec. V, Fig. 4).

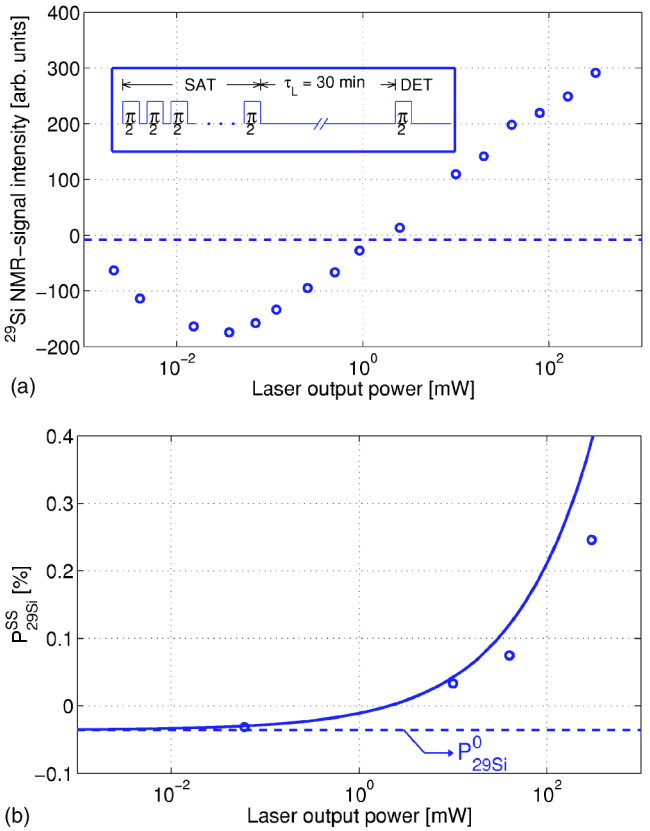

FIG. 1. (Color online) Optical pumping data as a function of laser power for the ^{29}Si-enriched sample after irradiation with linearly polarized laser light of wavelength $\lambda_{\mathrm{photon}} = 1024.8$ nm at $T = 4$ K and $B_0 = 7$ T. (a) ^{29}Si NMR-signal intensity after 30 min of laser irradiation. The dashed line represents the ^{29}Si NMR-signal intensity after 30 min in the dark. The NMR-signal intensity is given by the area underneath the real part of the Fourier transform of the free induction decay (FID). (b) Steady-state ^{29}Si polarization as a function of laser power. The solid line represents our theoretical model which will be derived in Sec. IV B. The dashed line corresponds to the thermal-equilibrium polarization $P^0_{29\mathrm{Si}}$ at $T = 4$ K and $B_0 = 7$ T. The actual laser power penetrating into the sample is estimated to be $40 \pm 10\%$ of the displayed laser output power. The maximum laser power used for the experiments is about 500 mW because the cooling capability of the system is not sufficient to keep the temperature at $T = 4$ K when higher laser powers are used.

A. Experimental data

Figure 1(a) displays the ^{29}Si NMR-signal intensity as a function of laser power after optical pumping for a time $\tau_L = 30$ min. The experimental sequence is

$$\mathrm{SAT} - \tau_L - \mathrm{DET}, \tag{1}$$

with SAT a saturation NMR pulse sequence, which removes any existing ^{29}Si spin polarization and which consists of a train of $\pi/2$-pulses which are separated by a time longer than the ^{29}Si nuclear phase relaxation time, with τ_L the laser

irradiation time, and with DET the detection of the ^{29}Si NMR signal with a $\pi/2$-pulse [see inset to Fig. 1(a)]. The data are reproducible (changes of less than 20% for separate cooldowns of the setup) and the data are not affected by the presence of laser light during data acquisition.

We have performed longer optical pumping experiments ($\tau_L \approx 50$ h) to derive the steady-state ^{29}Si polarization $P_{29\mathrm{Si}}^{\mathrm{SS}}$ as a function of laser power. The results are presented in Fig. 1(b). To obtain the steady-state polarization, the buildup of ^{29}Si polarization is probed at regular intervals (2 to 4 h) during the irradiation time τ_L by sending very small tip-angle pulses (5° or below). It is assumed that the buildup of the ^{29}Si polarization toward its steady-state value $P_{29\mathrm{Si}}^{\mathrm{SS}}$ is characterized by a single time constant T_1^{Si}. A curve fit through the probing data provides the values of $P_{29\mathrm{Si}}^{\mathrm{SS}}$ (and T_1^{Si}) presented in Fig. 1(b). Since the irradiation time τ_L is shorter than T_1^{Si}, steady state is not reached within the duration of the experiment. However, the irradiation time is long enough to allow a reliable curve fit through the probing data.

The largest value of $P_{29\mathrm{Si}}^{\mathrm{SS}}$ we have recorded is 0.25% [see data point at $P_{\mathrm{laser}}=300$ mW in Fig. 1(b)]. Our maximum polarization is therefore a factor of 7 larger than the thermal-equilibrium polarization $P_{29\mathrm{Si}}^{0}$ and nearly an order of magnitude larger than the previous optical-pumping record.[10]

The conversion from NMR-signal intensity I_T to spin polarization P_T, necessary for the derivation of $P_{29\mathrm{Si}}^{\mathrm{SS}}$, is temperature dependent and is based on the following formula:

$$P_T = I_T / I_{300\ \mathrm{K}} \times Q_{300\ \mathrm{K}} / Q_T \times P_{300\ \mathrm{K}}, \tag{2}$$

with Q_T the Q-factor of the NMR probe at the given temperature, $I_{300\ \mathrm{K}}$ the experimentally determined thermal-equilibrium NMR-signal intensity at room temperature, and $P_{300\ \mathrm{K}}$ the corresponding theoretically-calculated spin polarization at room temperature. It has been verified that with our setup and under thermal-equilibrium circumstances, the polarization derived from Eq. (2) is close to the actual polarization over the temperature range of $T=4-300$ K. When determining $P_{29\mathrm{Si}}^{\mathrm{SS}}$ based on Eq. (2) for the optical pumping experiments of Fig. 1(b), the assumption is made that the laser-power density and therefore the ^{29}Si signal intensity and polarization are uniform over the sample volume. At $T=4$ K and $\lambda_{\mathrm{photon}}=1024.8$ nm the absorption length in silicon is $l_{\mathrm{abs}} \approx 20$ mm.[21] This length is large compared to the sample depth of $t \approx 5$ mm. The laser power is therefore fairly constant over the sample depth. Over the sample cross section, the laser beam has a Gaussian beam profile. The beam diameter at the sample surface is estimated to be 5 ± 1 mm. The laser power is therefore varying over the sample cross section. It can be verified however after the discussion in Sec. IV B that the uniformity assumption results in an underestimation of $P_{29\mathrm{Si}}^{\mathrm{SS}}$ with less than a factor of 2.

Comparison of the steady-state data set of Fig. 1(b) with the 30-min data set of Fig. 1(a) shows that T_1^{Si} varies with laser power. We derive this by considering that the polarization buildup is linearly proportional to $P_{29\mathrm{Si}}^{\mathrm{SS}}/T_1^{\mathrm{Si}}$ as long as the irradiation time is short compared to T_1^{Si}. This is the case for the 30-min data set. The initial negative increase in the 30-min data set therefore reflects a decrease in T_1^{Si}: T_1^{Si} is about 1200 h in the dark and has decreased to 65 h at 50 μW. This decrease of T_1^{Si} with increasing laser power is expected as more electronic carriers are created which can relax the nuclear spin system. At higher laser powers there is a slow increase in T_1^{Si} with increasing laser powers, which is currently not understood.

B. Theoretical model

The observed dynamic nuclear polarization (DNP) is due to cross relaxation of the ^{29}Si nuclear spins with non-thermal electron spins (Overhauser effect).[22] The effect of holes will be neglected because of the small hyperfine interaction of holes, which results from the purely p-type nature of the hole wave function in the valence band of silicon.[23] The ^{29}Si polarization induced by non-thermal free electron spins is first determined.

The rate equation for the free-electron spin polarization P_e, assuming very weak cross-relaxation processes, is

$$\frac{dP_e}{dt} = -\frac{(P_e - P_e^0)}{\tau_e^s}, \tag{3}$$

with P_e^0 the thermal-equilibrium free-electron spin polarization and τ_e^s the free-electron spin relaxation time. At $T=4$ K there are no free electrons. When optically injecting free electrons with a lifetime τ_e and with a spin polarization P_e^{inj}, the deviation from equilibrium of the steady-state free-electron spin polarization P_e^{SS} is therefore given by

$$\Delta P_e^{\mathrm{SS}} = P_e^{\mathrm{SS}} - P_e^0, \tag{4}$$

$$= (P_e^{\mathrm{inj}} - P_e^0) \int_0^\infty \exp(-t/\tau_e^s) \frac{\exp(-t/\tau_e)}{\tau_e} dt,$$

$$= \Delta P_e^{\mathrm{inj}} \frac{\tau_e^s}{\tau_e^s + \tau_e}. \tag{5}$$

Since the electron spin polarization upon injection is zero (linearly polarized light), Eq. (5) reduces to

$$\Delta P_e^{\mathrm{SS}} = -P_e^0 \frac{\tau_e^s}{\tau_e^s + \tau_e}. \tag{6}$$

The generation rate of free electrons and holes is assumed to be constant over the sample volume, as mentioned before. The generated free electrons and holes form free excitons[24] which get trapped at the neutral phosphorus atoms, which are the dominant dopants in the ^{29}Si-enriched sample.[25–27] Recombination of the donor-bound excitons (eeh-complex) takes place via an Auger process, whereby one electron of the eeh-complex recombines with the hole and the energy freed in the recombination process excites the second electron high in the conduction band.[28] The phosphorus atom is now ionized but will recapture a free electron to become neutral again.

The density of free electrons and free holes increases with laser power as

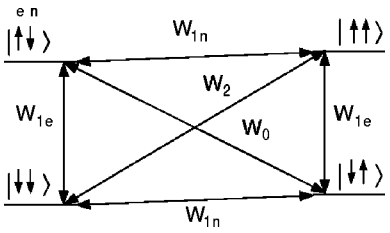

FIG. 2. Energy diagram for a system of one electron spin and one ^{29}Si nuclear spin in the presence of a magnetic field B_0. The notation $|\uparrow\uparrow\rangle$ represents $|$electron spin, nuclear spin$\rangle$. The lowest energy state is $|\downarrow\downarrow\rangle$ because the gyromagnetic ratio of the electron and the ^{29}Si nucleus are both negative. All spin transitions are indicated and labeled with the corresponding transition probability W_i, with i the net number of spin flips of the transition.

$$n_h \approx n_e \propto \sqrt{P_{\text{laser}}}, \tag{7}$$

because the free exciton formation is the dominant recombination process. This implies that the free electron lifetime τ_e decreases with increasing laser power as

$$\tau_e \propto 1/n_e \propto 1/\sqrt{P_{\text{laser}}}. \tag{8}$$

For the power range of our experiments the lifetime varies from $\tau_e \approx 500$ μs to $\tau_e \approx 1.5$ μs.

The dominant source of free-electron spin relaxation for our moderately doped ^{29}Si-enriched sample and for our operating regime is expected to be free-electron scattering with phonons (phonons modulate the crystal field, which then perturbs the electron's orbit; due to the electron spin-orbit interaction, the electron spin can be flipped).[29–32] The free-electron spin relaxation time at $T=4$ K and $B_0=7$ T is estimated to be on the order of $\tau_e^s=1-100$ ns.[29–32] The spin relaxation time τ_e^s is independent of laser power, as long as the temperature is constant and the spin relaxation due to other injected electronic carriers is negligible. The latter is expected to be the case since the density of unpaired carriers upon laser irradiation is small (the free electron density, which is the largest electronic density for the ^{29}Si-enriched sample over the power range of our experiments, is about 10^{12} cm^{-3} at our maximum laser power).

Since $\tau_e > \tau_e^s$ for our operating regime, Eq. (6) reduces to

$$\Delta P_e^{\text{SS}} = -P_e^0 \frac{\tau_e^s}{\tau_e} \propto \sqrt{P_{\text{laser}}}, \tag{9}$$

which shows that P_e^{SS} depends strongly on laser power.

The variation of $P_{29\text{Si}}^{\text{SS}}$ with P_e^{SS} then depends on the electron-nucleus cross-relaxation process and on the presence of other (parasitic) nuclear relaxation processes. Figure 2 gives the general energy diagram for a system of one electron and one nucleus, with all spin transitions indicated and labeled with the corresponding transition probabilities W_i, with i the net number of spin flips of the transition. The transition probability W_{1e} is much larger than all other transition probabilities ($\tau_e^s \ll T_1^{\text{Si}}$), such that the electron spin polarization does not depend on the nuclear spin polarization,

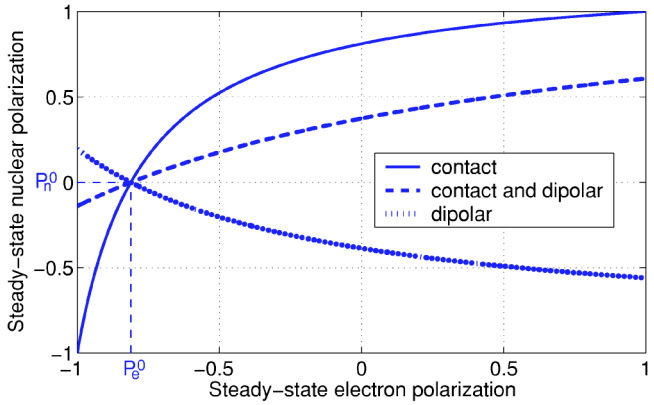

FIG. 3. (Color online) $P_{29\text{Si}}^{\text{SS}}$ as a function of P_e^{SS} for a pure contact hyperfine interaction (only $w_0 \neq 0$), for a hyperfine interaction such that $\{w_0:w_1:w_3\}=\{1:1:0\}$, and for a pure dipolar hyperfine interaction with $\{w_0:w_1:w_3\}=\{1:3:6\}$. The curves are valid for silicon at $T=4$ K and $B_0=7$ T and in the absence of nuclear spin relaxation due to (parasitic) electron spin reservoirs with thermal spin polarization (leakage factor $f=1$) (Ref. 34). The horizontal and vertical dashed lines indicate, respectively, the thermal nuclear-spin and the thermal electron-spin polarization.

as assumed when deriving Eq. (5). The steady-state nuclear spin polarization P_n is determined by the following rate equation, derived from Fig. 2:

$$\frac{dn^+}{dt} = e^+n^-W_0^{+-} - e^-n^+W_0^{-+} + e^-n^-W_2^{--} - e^+n^+W_2^{++} + n^-W_{1n}^- - n^+W_{1n}^+ = 0, \tag{10}$$

with $P_n=(n^+-n^-)/(n^++n^-)$, with e^+ (e^-) the probability that the electron spin is up (down) and n^+ (n^-) the probability that the nuclear spin is up (down), and with W_0^{+-} the probability of a W_0 transition starting from the spin state $|\uparrow\downarrow\rangle$. Instead of W_i, the following notations are also used:

$$w_0 = W_0^{+-} \exp[\hbar(\gamma_e - \gamma_{\text{Si}})B_0/kT], \tag{11}$$

$$w_1 = W_{1n}^+ \exp(\hbar\gamma_{\text{Si}}B_0/kT), \tag{12}$$

$$w_2 = W_2^{++} \exp[\hbar(\gamma_e + \gamma_{\text{Si}})B_0/kT], \tag{13}$$

with γ_{Si} and γ_e the ^{29}Si and electron gyromagnetic ratio, respectively, $\hbar$ the Planck constant, and k the Boltzmann constant. The value of P_n, which can be derived from Eq. (10), is therefore a function of the electron spin polarization, temperature, magnetic field, nuclear isotope, and the relative values of the transition probabilities w_i.

Figure 3 displays $P_{29\text{Si}}^{\text{SS}}$ as a function of P_e^{SS} at $T=4$ K and $B_0=7$ T and, respectively, for a pure contact hyperfine interaction (only $w_0 \neq 0$), for a contact hyperfine interaction together with a dipolar interaction of the type which induces nuclear spin flips only ($w_0 \neq 0, w_1 \neq 0$), and for a pure dipolar hyperfine interaction, in which case the simultaneous flipping of electron and nuclear spins in the same direction is more probably than the flipping in opposite directions ($w_0 < w_2$).[17,22,33] Since the induced nuclear polarization enhancements in our optical pumping experiments are positive

[see Fig. 1(b)], it can be concluded from Fig. 3 that the dominant hyperfine interaction is a contact hyperfine interaction, with potentially dipolar interactions of the type which only flip the nuclear spin.

For very small values of $P_{29\mathrm{Si}}^{\mathrm{SS}}$, the deviation $\Delta P_{29\mathrm{Si}}^{\mathrm{SS}}$ is linearly proportional to the deviation ΔP_e^{SS}. In the case of a pure contact hyperfine interaction, the dependence is (see Fig. 3)

$$\Delta P_{29\mathrm{Si}}^{\mathrm{SS}} = 3\Delta P_e^{\mathrm{SS}}. \tag{14}$$

The general relationship, for small values of $P_{29\mathrm{Si}}^{\mathrm{SS}}$, is then given by

$$\Delta P_{29\mathrm{Si}}^{\mathrm{SS}} = 3f_{\mathrm{tot}}\Delta P_e^{\mathrm{SS}}, \tag{15}$$

with f_{tot} the total leakage factor, representing both loss of polarization because the nuclear spins interact with (parasitic) electronic reservoirs with thermal spin polarization[17,34] and loss of polarization because the hyperfine interaction is not purely of the contact type. Inserting Eq. (9) in Eq. (15) then results in the following dependence, valid for our operating regime:

$$\Delta P_{29\,\mathrm{Si}}^{\mathrm{SS}} = -3f_{\mathrm{tot}}P_e^0\frac{\tau_e^s}{\tau_e} \propto \sqrt{P_{\mathrm{laser}}}. \tag{16}$$

We have used the model of Eq. (16) to fit the data of Fig. 1(b). The proportionality factor is determined by the requirement that the 30-min data set of Fig. 1(a) and the steady-state data set of Fig. 1(b) have a zero-crossing of signal intensity and polarization, respectively, at the same laser power. It can be seen that the model is in very good agreement with the data, especially if one considers that the laser power covers more than three orders of magnitude.

The uncertainty in the free-electron spin relaxation time (τ_e^s=1–100 ns, see before) results in an uncertainty in the total leakage factor f_{tot}: the leakage factor is f_{tot}=0.02 for τ_e^s=100 ns and f_{tot}=1 for τ_e^s=2 ns. Since the maximum value of the fitting factor is $f_{\mathrm{tot,max}}$=1 by definition, it follows from our data modeling that the free-electron spin relaxation time must be $\tau_e^s \geqslant 2$ ns. From Fig. 3 and from the meaning of the leakage factor, we then derive that the maximum achievable ^{29}Si polarization for f_{tot}=0.02–1 is $P_{29\mathrm{Si}}^{\mathrm{SS}}$=2%–83% when linearly polarized light is used. This maximum ^{29}Si polarization is obtained when $\tau_e < \tau_e^s$, which requires that the laser power is significantly increased [see Eq. (8)]. The laser power cannot be increased beyond about 500 mW with our setup because the cooling capability of the system is not sufficient to keep the temperature at T=4 K when higher powers are used. However, the laser wavelength also affects the value of τ_e as will be discussed in Sec. V.

C. Responsible electronic reservoir

The theoretical model of Eq. (16) fits our data of Fig. 1(b) very well. The electronic source responsible for DNP must therefore be the free electron reservoir or a reservoir which has the same dependence on laser power as the free electron reservoir. We have also derived that the hyperfine interaction of the responsible reservoir must be of the contact type with possibly some dipolar interaction of the type which induces nuclear spin flips only. Both the free electron reservoir and the phosphorus donor-electron reservoir fulfill these requirements. The spin polarization of the latter is the same as the spin polarization of the free electron reservoir, which is the result of an exchange process between the donor-bound electrons and the free electrons.[30,35,36]

In order to further identify the electronic reservoir responsible for DNP, our experimental values of T_1^{Si} are compared with theoretical predictions, if available. The free electron reservoir is unlikely to be the source of DNP as it contains too few free electrons to create significant nuclear polarization within the duration of our experiments ($T_{1,\mathrm{theor}}^{\mathrm{Si}} \gg T_{1,\mathrm{exp}}^{\mathrm{Si}}$).[22] The same applies to the free exciton reservoir, whose density is even smaller than the free electron reservoir. The phosphorus donor-electron reservoir is a more likely candidate as the density of (neutral) phosphorus atoms is about three orders of magnitude larger than the largest free electron density for our experiments. However, nuclear relaxation by neutral donors is also available in the dark and known modulation processes which become active upon light irradiation (for example modulation due to the exchange process between donor electrons and conduction electrons) are too slow to improve the nuclear relaxation.[37] Since theoretical investigations of the nuclear relaxation by neutral (phosphorus) donors have not been made yet for our operating regime, it is premature to judge the importance of the donor-electron reservoir based on T_1^{Si} values. For the other electronic reservoirs in the system, like the donor-bound exciton reservoir and reservoirs related to paramagnetic defects, no theoretical models of nuclear relaxation are known either.

To identify the electronic reservoir which is the source of DNP in bulk silicon, it is therefore necessary that the theoretical analysis of electron-nucleus cross-relaxation processes is extended to the high magnetic field and low temperature regime.[35]

V. RESULTS AS A FUNCTION OF LASER WAVELENGTH

When exciting far above the band gap the absorption length shortens such that high free electron densities are created close to the exposed sample surface, which results in short free electron lifetimes [see Eq. (8)]. The induced ^{29}Si polarization therefore increases and gets closer to the maximum achievable ^{29}Si polarization, provided that the free-electron spin relaxation time is not degraded by exciting high above the band gap.

A. Experimental data

Figure 4 shows the ^{29}Si NMR-signal intensity as a function of laser wavelength after optical pumping of the ^{29}Si-enriched sample for a time τ_L=25 min with different laser powers at T=4 K and B_0=7 T. The experimental sequence is again "SAT-τ_L-DET." The data vary rather continuously with wavelength, except at a few wavelengths where abrupt changes are observed (E_{photon}=1.17 and 1.21 eV).

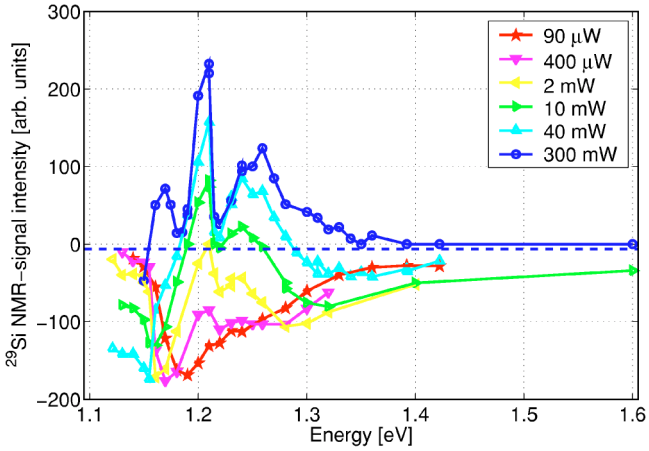

FIG. 4. (Color online) ^{29}Si NMR-signal intensity as a function of laser wavelength for the ^{29}Si-enriched sample after 25 min of laser irradiation with linearly polarized laser light at $T=4$ K and $B_0=7$ T. The different curves are the results for different laser powers and the data points are connected for better clarity. The dashed line represents the ^{29}Si NMR-signal intensity after 25 min in the dark. The NMR-signal intensity is given by the area underneath the real part of the Fourier transform of the FID.

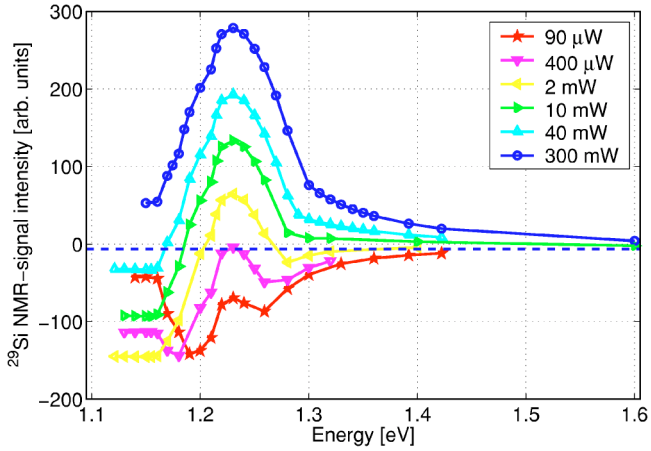

FIG. 5. (Color online) Theoretical calculation of the ^{29}Si NMR-signal intensity as a function of laser wavelength for the ^{29}Si-enriched sample after 25 min of laser irradiation with linearly polarized light at $T=4$ K and $B_0=7$ T. The calculation is made for a limited number of wavelength and power combinations (see data points) and the data points for a particular power level are connected for better clarity. The dashed line represents the ^{29}Si NMR-signal intensity after 25 min in the dark. The calculations are based on the absorption-length data of Ref. 21 and the experimental data of Fig. 1(a).

B. Theoretical model

We establish a first-order model which predicts the ^{29}Si NMR-signal intensity as a function of laser wavelength. The model is based on the data of Fig. 1(a), which determine the relation between the ^{29}Si NMR-signal intensity and the electron-hole generation rate, and on the absorption-length data of Ref. 21, which determine the relation between the electron-hole generation rate and the laser wavelength.

For $E_{\text{photon}}>1.3$ eV, extrapolation of the absorption-length data of Ref. 21 is required. The extrapolations are made based on the following dependence which is valid for indirect transitions:[38]

$$1/l_{\text{abs}} \propto (E_{\text{photon}} - E_g - E_{\text{phonon}})^2. \tag{17}$$

Below the band gap the absorption length is sample-specific and therefore the lowest energy to which our theoretical model is applied is $E_{\text{photon}}=1.16$ eV. The electron-hole generation rate $g_{e,h}$ per unit length as a function of sample depth x is then proportional to

$$g'_{e,h}(x) \propto \frac{P_{\text{laser}}}{l_{\text{abs}}} \exp\left(-\frac{x}{l_{\text{abs}}}\right). \tag{18}$$

The ^{29}Si NMR-signal intensity per unit length corresponding to the electron-hole generation rate per unit length is derived from the data in Fig. 1(a). These data need to be extrapolated as well. The extrapolation to lower powers connects the value at the lowest laser power to the value in the dark. The exact shape of this extrapolation does not influence the resulting model very much for our power range and wavelength range. The extrapolation of the data to higher powers is made as a linear extension of the data points of Fig. 1(a). This extension is a rather arbitrary choice. The choice of extrapolation has a quantitative effect on the model for our power range and for photon energies larger than $E_{\text{photon}}=1.21$ eV. The resulting absorption-length model should therefore only be used qualitatively for $E_{\text{photon}}>1.21$ eV.

Integration of the ^{29}Si NMR-signal intensity per unit length over the sample thickness then gives the expected value of the ^{29}Si NMR-signal intensity for a given laser wavelength and laser power. The results are displayed in Fig. 5.

The general shape of the curves of Fig. 5 can intuitively be understood as follows. At photon energies $E_{\text{photon}}<1.21$ eV the absorption length is larger than the sample thickness ($l_{\text{abs}}>t=5$ mm).[21] The photon absorption is therefore nearly uniform over the sample volume and the ^{29}Si signals follow the dependence of Fig. 1(a) with increasing photon energy. At photon energies $E_{\text{photon}}>1.23$ eV the absorption is nonuniform over the sample depth ($l_{\text{abs}}\leqslant 2.5$ mm).[21] The ^{29}Si signals decrease with increasing photon energy because the ^{29}Si signal intensity increases less-than-linearly with photon absorption [see Sec. IV and Fig. 1(a)] and because for high photon absorption the ^{29}Si signals are positive while for low photon absorption the ^{29}Si signals are negative, such that cancellation of signals can occur. At even higher photon energies, when the photons are absorbed very close to the sample surface, such that a large part of the sample volume is not affected by the laser light, the values of the ^{29}Si signals tend to the value in the dark.

Except for the abrupt changes in the experimental data, the theoretical curves of Fig. 5 are in qualitative agreement with the experimental curves of Fig. 4. This agreement supports our model of nonuniform ^{29}Si polarization buildup over the sample depth when exciting high above the band gap. As mentioned before, the agreement above $E_{\text{photon}}=1.25$ eV is not expected to be quantitative as it is based on an extrapo-

lation of the experimental data. Furthermore the theoretical model is a first-order approximation since second-order effects like diffusion of free electrons, increased carrier recombination near the sample surfaces and nuclear spin diffusion are not included.

C. Special features

There are two special features in the experimental data of Fig. 4 which are not explained by the theoretical absorption-length model of Sec. V B. The features consist of a sudden drop in ^{29}Si signal intensity at a particular photon energy and a slow recovery toward theoretical expectations beyond this photon energy. The feature starting right above $E_{\text{photon}}=1.17$ eV is only present for the highest laser power ($P_{\text{laser}}=300$ mW). The feature starting right above $E_{\text{photon}}=1.210$ eV is present for all power levels and the drop in signal intensity is more abrupt for the higher laser powers.

We remark that the onset of TA-phonon-assisted band-to-band transitions and the onset of TO-phonon-assisted band-to-band transitions start with the creation of free excitons at $E_{\text{photon}}=1.174$ and 1.213 eV, respectively.[18] These energies correspond to the photon energies at which the abrupt changes are observed, which suggests that the creation of high concentrations of (low-energy) free excitons is destructive for the dynamic-nuclear-polarization mechanism. It is also noted that the generation of free excitons becomes less important at higher photon energies relative to the generation of free electron-hole pairs, which could explain why the agreement of the experimental data with the theoretical model is restored for higher photon energies.[38,39]

Similar features have been observed in optical pumping experiments with indium phosphide (InP) and GaAs, but the features are not fully understood either.[40,41]

D. Experimental data for a thinner sample

The experimental data of Fig. 4 are consistent with the absorption-length model of Fig. 5. The small signals far above the band gap, obtained after $\tau_L=25$ min of laser irradiation, are therefore expected to be the sum of a large and positive ^{29}Si signal close to the exposed surface, a negative ^{29}Si signal deeper in the sample and hardly any signal from the bulk of the sample, where the nuclear spin relaxation time is very long. However, the small signals far above the band gap could also be caused by a breakdown of the DNP mechanism. To exclude this possibility, additional experiments have been performed in which only the signal of the ^{29}Si spins close to the exposed surface is measured. As we do not have imaging capabilities in our setup, we have cut a slice of 500 μm from the original ^{29}Si-enriched sample to this purpose.

The average ^{29}Si NMR-signal intensities per unit volume after 25 min of laser irradiation at $T=4$ K and $B_0=7$ T are displayed in Fig. 6 for the 500 μm sample and the original 5 mm sample as a function of laser wavelength. At low photon energies ($E_{\text{photon}}<1.21$ eV) the two curves coincide. This is expected because the absorption length is longer than the sample thickness for both samples. Starting right above

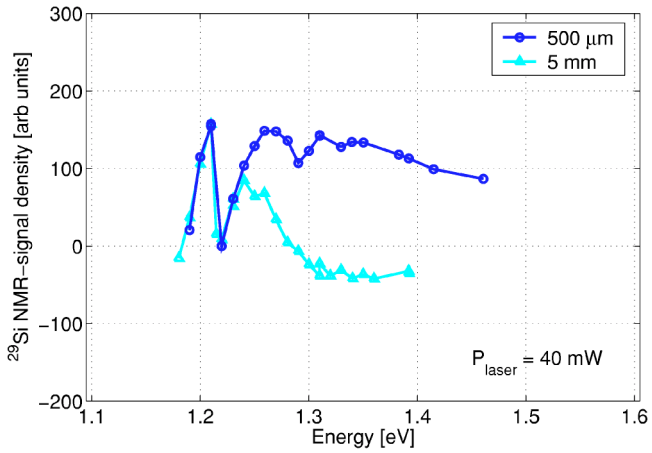

FIG. 6. (Color online) Average ^{29}Si NMR-signal intensity per unit volume as a function of laser wavelength after 25 min of laser irradiation with linearly polarized laser light at $T=4$ K and $B_0=7$ T. The curves are the results for the 5 mm thick ^{29}Si-enriched sample and for a 500 μm slice of the original sample. The data points are connected for better clarity. The NMR-signal intensity is given by the area underneath the real part of the Fourier transform of the FID.

$E_{\text{photon}}=1.21$ eV the special feature is observed. Beyond $E_{\text{photon}}=1.24$ eV ($l_{\text{abs}}=1.5$ mm)[21] the two curves start to deviate. The average signal intensity per unit volume for the 500 μm sample is positive and larger in absolute value than the average signal intensity per unit volume for the 5 mm sample. This indicates that in the 5 mm sample, signal cancellation occurs between the sample volume close to the surface and the remainder of the sample.

The experiments presented in Fig. 6 therefore confirm that the small signals at high photon energies in Fig. 4 are due to signal cancellation and not due to a breakdown of the DNP mechanism. The positive data for the thin sample at high photon energies also demonstrate that non-thermal electron spin polarizations can be preserved when exciting high above the band gap. This implies that the electron spin-orbit coupling is small enough such that the free-electron spin relaxation rate does not increase significantly when the free electron relaxes from high in the conduction band to the bottom of the conduction band. It is therefore very promising to continue the investigation of silicon optical pumping at high photon energies. Especially valuable will be experiments which determine the amount of steady-state ^{29}Si polarization, achievable close to the exposed surface at high photon energies. This can be done via experiments similar to the ones of Fig. 1(b).

VI. RESULTS AS A FUNCTION OF TEMPERATURE AND MAGNETIC FIELD

Experiments are performed to determine the most favorable conditions of temperature and magnetic field to create high ^{29}Si polarizations.

A. Temperature dependence

The optical pumping experiments to determine the effect of temperature are performed at $B_0=7$ T with the

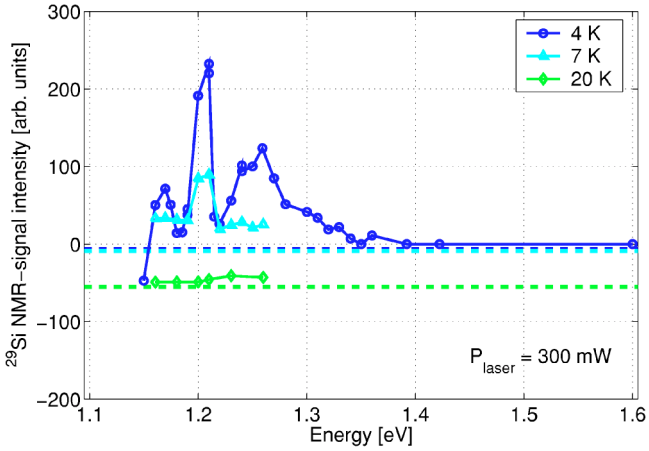

FIG. 7. (Color online) ^{29}Si NMR-signal intensity as a function of laser wavelength for the ^{29}Si-enriched sample after 25 min of laser irradiation with linearly polarized light at $B_0=7$ T. The different curves are the results for different temperatures and the data points are connected for better clarity. The dashed lines represent the ^{29}Si NMR-signal intensity after 25 min in the dark for the respective temperatures. The NMR-signal intensity is given by the area underneath the real part of the Fourier transform of the FID.

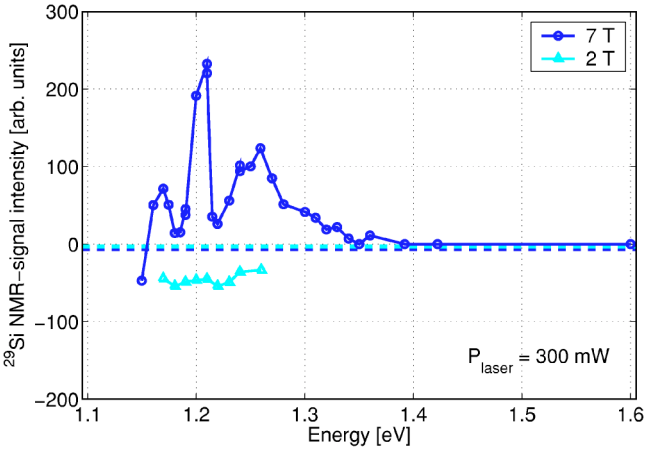

FIG. 8. (Color online) ^{29}Si NMR-signal intensity as a function of laser wavelength for the ^{29}Si-enriched sample after 25 min of laser irradiation with linearly polarized laser light at $T=4$ K. The different curves are the results for different magnetic fields and the data points are connected for better clarity. The dashed lines represent the ^{29}Si NMR-signal intensity after 25 min in the dark for the respective magnetic fields. The NMR-signal intensity is given by the area underneath the real part of the Fourier transform of the FID.

^{29}Si-enriched sample. Figure 7 shows the ^{29}Si NMR-signal intensity as a function of laser wavelength after optical pumping for a time $\tau_L=25$ min at $T=4$, 7, and 20 K. The ^{29}Si signals at $T=7$ K have decreased compared to the ^{29}Si signals at $T=4$ K. At $T=20$ K, the ^{29}Si signals are no longer positive. According to our model of Eq. (16) [see Fig. 1(b)], the steady-state ^{29}Si polarization will therefore be equal to or smaller in absolute value than the thermal-equilibrium polarization at $T=20$ K. The lack of positive signals at $T=20$ K therefore indicates that the DNP effect has significantly decreased.

Since an increase in temperature has a strong and destructive effect on the DNP mechanism, it is expected that decreasing the temperature to below $T=4$ K will increase the maximum achievable ^{29}Si polarization.

B. Magnetic field dependence

The optical pumping experiments to determine the effect of magnetic field are performed at $T=4$ K with the ^{29}Si-enriched sample. Figure 8 shows the ^{29}Si NMR-signal intensity as a function of laser wavelength after optical pumping for a time $\tau_L=25$ min at $B_0=7$ and 2 T. At $B_0=2$ T the ^{29}Si signals are no longer positive. As mentioned before, this is a clear indication that the DNP effect has significantly decreased compared to at $B_0=7$ T.

Since a decrease in magnetic field has a strong and destructive effect on the DNP mechanism, it is expected that increasing the magnetic field above $B_0=7$ T will increase the maximum achievable ^{29}Si polarization.

VII. RESULTS AS A FUNCTION OF DOPING

The effect of doping and dislocations on the maximum achievable ^{29}Si polarization cannot be predicted very accurately because the details of the DNP mechanism for our operating regime are not known yet. Experiments are therefore performed to increase our insight in the role of doping.

As mentioned before, the production of ^{29}Si-enriched silicon is still at the research stage. For this work, only one ^{29}Si-enriched sample has been available. To investigate the effect of doping, we have therefore performed experiments with naturally-abundant silicon samples. The specifications of these samples are given in Table I. Samples 1, 2, 4, and 5 consist of a stack of eight 8×8 mm^2 pieces of single-crystal silicon wafer (500 μm thick) with orientation [100]. Sample 3 is a bulk piece of similar dimensions.

Optical pumping experiments are performed at $T=4$ K and $B_0=7$ T with laser light of wavelength $\lambda_{photon}=1024.8$ nm and at a laser power of $P_{laser}=300$ mW. The chosen laser settings are expected to produce the largest ^{29}Si signals (see Fig. 4). This is desired because the ^{29}Si density in naturally-abundant silicon is 20 times smaller than in the ^{29}Si-enriched sample, resulting in 20 times smaller NMR signals. It has still been necessary to increase the irradiation time to $\tau_L=8$ h to allow single-shot detection. The resulting ^{29}Si NMR-signal intensities are shown in Fig. 9 as

TABLE I. Naturally-abundant silicon samples.

	Doping level (cm^{-3})	Doping atom	Quality
1	$1-5\times10^{15}$	Phosphorus	Prime
2	$4-10\times10^{14}$	Phosphorus	Test
3	$<5\times10^{13}$	—	Very pure, high quality
4	$2-4\times10^{15}$	Boron	Test
5	$1-3\times10^{15}$	Boron	Test

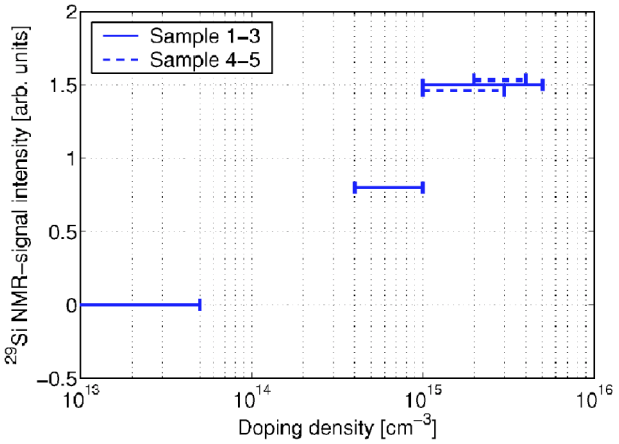

FIG. 9. (Color online) ^{29}Si NMR-signal intensity as a function of doping density for naturally-abundant silicon samples after 8 h of laser irradiation with linearly polarized light of wavelength $\lambda_{photon}=1024.8$ nm. The experiments are performed at $T=4$ K and $B_0=7$ T and with a laser power of $P_{laser}=300$ mW. The different line styles represent different doping types. The samples are described in Table I. The NMR-signal intensity is given by the resonance-peak height of the real part of the Fourier transform of the FID.

a function of doping density. The signals are positive, which indicates that there is a dynamic-nuclear-polarization effect, just like in the ^{29}Si-enriched sample.

For the *n*-type samples, the signal increases with increasing doping density. This implies that either phosphorus-related electronic reservoirs interact directly with the ^{29}Si nuclei or that the phosphorus doping affects the ^{29}Si nuclei indirectly, by influencing the electronic reservoirs with which the nuclei interact. Whether the observed ^{29}Si signal increase is mainly due to an increase in the steady-state ^{29}Si polarization or also partially due to a decrease in the nuclear-spin relaxation time is uncertain. Longer experiments, which determine the values of both P_{29Si}^{SS} and T_1^{Si}, need to be performed to find out.

No difference is observed between the ^{29}Si signal for an *n*-type sample and the ^{29}Si signal for a *p*-type sample with the same doping density. Since neutral acceptors are about ten times less effective in interacting with nuclei than neutral donors,[23] this suggests that the nuclear polarization is not induced at neutral dopants, but for example at dopants with a bound exciton or, as mentioned before, via interaction with other electronic reservoirs which are affected by the dopant density.

It is also noted that the ^{29}Si signals of the naturally-abundant samples, which are obtained after 8 h of irradiation, correspond to polarizations which are an order of magnitude smaller than the polarizations produced in the ^{29}Si-enriched sample after the same irradiation time under the same conditions. This could mean that the dislocations, which are present in the ^{29}Si-enriched sample, have an impact on the optical pumping mechanism. But the smaller signals could also be caused by a slower nuclear spin relaxation process in the naturally-abundant samples due to the smaller ^{29}Si isotopic content.[37,42]

In conclusion, increasing the doping density either increases the steady-state ^{29}Si polarization or decreases the energy relaxation time. A decrease in T_1^{Si} would be beneficial for the experimental investigations, because certain experiments, like the ones to determine the steady-state ^{29}Si polarization, are very challenging due to the long duration of the experiments. It is therefore valuable to investigate the effect of doping in more detail. Such a study may also help to identify the electronic reservoir responsible for the induced ^{29}Si polarization.

VIII. CONCLUSIONS

We have performed optical pumping experiments with bulk silicon at the liquid helium temperature and at high magnetic field field ($B_0=7$ T) and we have observed ^{29}Si polarization enhancements both in ^{29}Si-enriched and naturally-abundant silicon. We have improved the previous optical-pumping record with nearly an order of magnitude, up to ^{29}Si polarizations of 0.25%.

We have derived a theoretical model which explains the observed dependence of the induced ^{29}Si polarization on laser power. This model predicts that at $T=4$ K and $B_0=7$ T the maximum achievable ^{29}Si polarization for the ^{29}Si-enriched sample, when exciting with linearly polarized light of wavelength $\lambda_{photon}=1024.8$ nm, is 2%–83%. The uncertainty in the prediction is due to uncertainty in the free-electron spin relaxation time ($\tau_e^s=2-100$ ns). To achieve the maximum predicted ^{29}Si polarization, significantly higher laser powers are required than is possible with our setup. We have demonstrated that high photon absorption can also be created close to the sample surface when exciting far above the band gap and that the dynamic-nuclear-polarization capabilities are well-preserved in this regime. If there would be no degradation of the dynamic-nuclear-polarization capabilities compared to excitation at $\lambda_{photon}=1024.8$ nm then, for a laser power of 300 mW, the maximum ^{29}Si polarization of $P_{29Si}^{SS\,max}=2\%$(predicted for $\tau_e^s=100$ ns) will be achieved when exciting at 1.38 eV, and the maximum ^{29}Si polarization of $P_{29Si}^{SS\,max}=83\%$ (predicted for $\tau_e^s=2$ ns) when exciting higher than the direct band gap of silicon. In the latter case the spin relaxation rate of the injected conduction electrons may have increased, which may reduce the achievable polarization maximum. We further expect from our investigations that decreasing the temperature and increasing the magnetic field will help to achieve high polarizations, potentially even higher than the above predicted values. Our findings therefore do not exclude yet that ^{29}Si polarizations close to 100% can be obtained with the optical pumping technique at temperatures above 1 K and magnetic fields below 20 T. Such achievements would be very important for the field of quantum computation.[6,7] Further optical pumping research in bulk silicon is therefore stimulated, and a focus on the determination of the ^{29}Si polarization, achieved close to the exposed sample surface when exciting far above the band gap, will be especially valuable.

We provide a probe to investigate the dynamic-nuclear-polarization mechanism in semiconductors in the high magnetic field and low temperature regime. In this regime, there are several details about the optical pumping mechanism in silicon as well as in GaAs which are not understood. The

exact electron-nucleus polarization transfer mechanism, for example, is not understood in detail. Neither are the special features observed when exciting above the band gap. A significant advantage of silicon in exploring these electron-nucleus interactions is its very simple nuclear spin system, which consists of only one active isotope, ^{29}Si, without a quadrupolar moment. However, silicon has the disadvantage of a very long nuclear spin relaxation time, which is on the order of tens to hundreds of hours in the ^{29}Si-enriched sample at liquid helium temperatures. This problem may be alleviated by increasing the doping density.

We have derived that in our operating regime, increasing the laser power increases the induced ^{29}Si polarization because it decreases the free electron lifetime. This result stimulates the investigation of optical pumping in other indirect band gap materials.

ACKNOWLEDGMENTS

The authors thank A. K. Paravastu for informative discussions and help with the experimental setup, Professor D. Snoke for advice on hermetic sealing, and H. Deng and T. D. Ladd for useful discussions. We are grateful to the IBM Almaden Research Center, San Jose, for lending us NMR spectroscopy equipment. The work at Stanford University was supported by DARPA under the QuIST initiative and the work at Keio University was supported in part by the Grant-in-Aid for Scientific Research Nos. 64076215 and 14076215 (semiconductor nanospintronics).

*Electronic address: anne.verhulst@imec.be
†Also at NTT Basic Research Laboratories, 3-1 Morinosato-Wakamiya, Atsugi-shi, Kanagawa 243-01, Japan.

[1] L. M. K. Vandersypen, M. Steffen, G. Breyta, C. S. Yannoni, M. H. Sherwood, and I. L. Chuang, Nature (London) **414**, 883 (2001).
[2] E. Knill, R. Laflamme, R. Martinez, and C. Negrevergne, Phys. Rev. Lett. **86**, 5811 (2001).
[3] F. Yamaguchi and Y. Yamamoto, Appl. Phys. A: Materials Science Processing **68**, No. 1, 1–8 (1999).
[4] D. G. Cory, R. Laflamme, E. Knill, L. Viola, T. F. Havel, N. Boulant, G. Boutis, E. Fortunato, S. Lloyd, R. Martinez, C. Negrevergne, M. Pravia, Y. Sharf, G. Teklemariam, Y. S. Weinstein, and W. H. Zurek, Fortschr. Phys. **48**, 875 (2000).
[5] B. E. Kane, Fortschr. Phys. **48**, 1023 (2000).
[6] B. E. Kane, Nature (London) **393**, 133 (1998).
[7] T. D. Ladd, J. R. Goldman, F. Yamaguchi, Y. Yamamoto, E. Abe, and K. M. Itoh, Phys. Rev. Lett. **89**, 017901 (2002).
[8] G. Lampel, Phys. Rev. Lett. **20**, 491 (1968).
[9] N. T. Bagraev, L. S. Vlasenko, and R. A. Zhitnikov, Zh. Eksp. Teor. Fiz. **71**, 952 (1976) [Sov. Phys. JETP **44**, 500 (1976)].
[10] N. T. Bagraev and L. S. Vlasenko, Fiz. Tverd. Tela (Leningrad) **24**, 3470 (1982) [Sov. Phys. Solid State **24**, 1974 (1982)].
[11] R. Tycko and J. A. Reimer, J. Phys. Chem. **100**, 13240 (1996).
[12] R. Tycko, S. E. Barrett, G. Dabbagh, L. N. Pfeiffer, and K. W. West, Science **268**, 1460 (1995).
[13] A. Imamoglu, E. Knill, L. Tian, and P. Zoller, Phys. Rev. Lett. **91**, 017402 (2003).
[14] K. M. Itoh, J. Kato, M. Uemura, A. K. Kaliteevskii, O. N. Godisov, G. G. Devyatych, A. D. Bulanov, A. V. Gusev, I. D. Kovalev, P. G. Sennikov, H.-J. Pohl, N. V. Abrosimov, and H. Riemann, Jpn. J. Appl. Phys., Part 1 **42**, 6248 (2003).
[15] A. S. Verhulst, D. Maryenko, Y. Yamamoto, and K. M. Itoh, Phys. Rev. B **68**, 054105 (2003).
[16] E. Abe, K. M. Itoh, J. Isoya, and S. Yamasaki, Phys. Rev. B **70**, 033204 (2004).
[17] A. S. Verhulst, Ph.D. thesis, Stanford Univerity, California, 2004.
[18] K. L. Shaklee and R. É Nahory, Phys. Rev. Lett. **24**, 942 (1970).
[19] Our calculations predict an increase of the indirect band gap with about 1 meV for the ^{29}Si-enriched sample due to the different isotopic content (see model in Ref. 20).
[20] S. Zollner, M. Cardona, and S. Gopalan, Phys. Rev. B **45**, 3376 (1992).
[21] G. G. Macfarlane, T. P. McLean, J. E. Quarrington, and V. Roberts, Phys. Rev. **111**, 1245 (1958).
[22] A. Abragam, *Principles of Nuclear Magnetism* (Oxford University Press, New York, 1999).
[23] R. G. Shulman and B. J. Wyluda, Phys. Rev. **103**, 1127 (1956).
[24] J. D. Cuthbert, Phys. Rev. B **1**, 1552 (1970).
[25] R. B. Hammond and R. N. Silver, Appl. Phys. Lett. **36**, 68 (1980).
[26] G. Schramm, Phys. Status Solidi A **125**, K113 (1991).
[27] T. M. Rice, in *Solid State Physics*, edited by H. Ehrenreich, F. Seitz, and D. Turnbull (Academic Press, London, 1977), Vol. 32, p. 1.
[28] W. Schmid, Phys. Status Solidi B **84**, 529 (1977).
[29] C. F. Young, E. H. Poindexter, G. J. Gerardi, W. L. Warren, and D. J. Keeble, Phys. Rev. B **55**, 16245 (1997).
[30] G. Feher and E. A. Gere, Phys. Rev. **114**, 1245 (1959).
[31] A. M. Portis, A. F. Kip, and C. Kittel, Phys. Rev. **90**, 988 (1953).
[32] Y. Yafet, in *Solid State Physics*, edited by F. Seitz and D. Turnbull (Academic Press, London, 1963), Vol. 14, pp. 67–96.
[33] N. T. Bagraev and L. S. Vlasenko, Zh. Eksp. Teor. Fiz. **75**, 1743 (1978) [Sov. Phys. JETP **48**, 878 (1978)].
[34] N. T. Bagraev, L. S. Vlasenko, and R. A. Zhitnikov, Pis'ma Zh. Eksp. Teor. Fiz. **23**, 639 (1976) [JETP Lett. **23**, 586 (1976)].
[35] D. K. Wilson and G. Feher, Phys. Rev. **124**, 1068 (1961).
[36] H. Honig and E. Stupp, Phys. Rev. Lett. **1**, 275 (1958).
[37] G. Lampel, Thèse de doctorat, Faculté des Sciences de Paris à Orsay, France, 1968.
[38] G. G. Macfarlane and V. Roberts, Phys. Rev. **97**, 1714 (1955).
[39] G. G. Macfarlane, T. P. McLean, J. E. Quarrington, and V. Roberts, Phys. Rev. **108**, 1377 (1957).
[40] C. A. Michal and R. Tycko, Phys. Rev. B **60**, 8672 (1999).
[41] A. K. Paravastu, S. E. Hayes, B. E. Schwickert, L. N. Dinh, M. Balooch, and J. A. Reimer, Phys. Rev. B **69**, 075203 (2004).
[42] W. E. Blumberg, Phys. Rev. **119**, 79 (1960).